YU ISSN 0015—3206
FZKAAA 17 (4) 465 (1985)

SEMICLASSICAL AND QUANTUM MECHANICAL ANALYSIS OF $^{16}O + {}^{28}Si$ ELASTIC SCATTERING

HALA M. KHALIL

University College for Girls, Ain Shams University, Heliopolis, Cairo, Egypt

and

MOSTAFA M. SHALABY and M. ABD EL-KERIEM

Ain Shams University, Faculty of Science, Phys. Dept., Cairo, Egypt

Received 1 September 1984

Revised manuscript received 28 January 1985

UDC 539.17

Original scientific paper

A search for the exact positions of the Regge poles of $^{16}O + {}^{28}Si$ elastic scattering S-matrix has been carried out using conventional optical model potential and over the energy range 33.16 MeV $\leq E_{Lab} <$ 55 MeV. The S-matrix was then parametrized in terms of these poles and an analytical expression for the corresponding deflection function $\Theta(l)$ was derived. $\Theta(l)$ clearly revealed semiclassical features in $^{16}O + {}^{28}Si$ elastic scattering as orbiting and rainbow phenomena for both real and complex potentials. Increasing the imaginary potential strength, dramatically shifts the Regge poles away from the real axis and the corresponding theoretical cross section shows a rapid (structureless) fall off beyond $\Theta_{cm} = 90^{\circ}$. This effect was also discussed in terms of the nearside/farside decomposition of the theoretical cross section.

1. Introduction

Measurements of $^{16}O + {}^{28}Si$ elastic scattering over the full angular range at energies 33 MeV $< E_{lab} <$ 55[1,2,3] are very interesting in heavy ion scattering. The most important feature of these data is the appearance of a smooth, exponential

fall in the cross section, at angles beyond the grazing (rainbow) angle, followed by a rapid oscillation of relatively large differential cross section in the backward hemisphere. This anomalous large angle scattering (ALAS) have been the subject of intensive theoretical investigations in recent years. At $E_{lab} = 55$ MeV the scattering has been analyzed by different methods such as: the conventional (LC) optical potential[4], modified optical model with l-dependence[5] or parity dependence[6] where more free parameters are involved. Other approaches are based on modification in the nuclear S-matrix elements, where $S(l)$ was taken as a combination of a background term (S_l^0) and another δS_l^0 term[7,8].

For more extensive optical model studies, we refer to the recent work of Kobos et al.[9], Kahana et al.[10] and Mermaz et al.[11]. The basic ingredient in the real nuclear potential they used is a »rise-dip« kink near the nuclear surface (5 fm $< r <$ 8 fm). It has been generated by Kobos et al.[9] using a double-folded (M3Y) potential supplemented by a phenomenological model-independent surface correction term, predominantly attractive and appearing to be greatest between 5 fm and 8 fm. Two corrections of surface derivative Woods-Saxon forms were added to a deep (700 MeV) real nuclear potential by Mermaz et al.[11], that together with their »extremely« transparent imaginary potential (with radius 1 fm and diffusivity $\simeq 0.025$) has successfully described ALAS. Kahana et al.[11] take the values of the real nuclear potential $V(r)$ at prespecified radii between 4 and 8 fm as »search parameters« in the fitting routine, with a constant potential for $r < 4$ fm and an exponential tail $e^{-r/a}$ for $r \geq 8$ fm.

In view of the above mentioned study, we suggest that a conventional optical model potential[12] will be suitable for further study as it reproduces ALAS and gives a reasonable fit over the whole angular range particularly at $E_{lab} = 33.16$ MeV. The study will be directed to interesting phenomena taking place in $^{16}O + {}^{28}Si$ elastic scattering; as the orbiting mechanism (near the grazing angular momentum) which was described by an almost but not complete destructive interference between orbital and background amplitudes[13]. Another interesting phenomenon is the nuclear rainbow appearing as smooth exponential fall of the cross section in the middle angular range (far from 0 and π where glory effect may take place). We try to explore the key physical process that is occuring in $^{16}O + {}^{28}Si$ elastic scattering, as orbiting and rainbow features, through the search for the exact location of Regge poles (singularities of the scattering matrix) and investigating behaviour of the classical deflection function near them. Also we display a direct connection between Regge poles and features of the cross section in an almost clear and reliable fashion.

2. *Preliminary review on semiclassical and quantum mechanical analysis*

The quantum mechanical scattering amplitude $f(\Theta)$ can be simply related to the classical deflection function ($\Theta(l) = 2\delta_l$) when the conditions for a semiclassical analysis of the quantum scattering are met:

$$f(\Theta) = \frac{1}{2ik} \sum_{l=0}^{\infty} (2l + 1)(e^{2i\delta_l} - 1) P_l(\cos\Theta). \tag{1}$$

The quantum mechanical cross section is:

$$\sigma(\Theta) = |f(\Theta)|^2. \tag{2}$$

In the semiclassical approximation of Ford and Wheeler[14], the phase shift δ_l is replaced by JWKB approximate values, the Legendre polynomial is replaced by its asymptotic expressions, and the summation is replaced by an integration ($\sum_l \to \int \mathrm{d}l$) then the integral is evaluated by the method of stationary phase (or by some other approximate method). The replacement of an infinite series of discrete terms by an integral of an analytic function is not novel and neither is the application of that procedure in physics. It was introduced by Poincaré[15] and Nicholson[16] and first applied in electromagnetic theory by Watson[17]. In quantum scattering theory, the Watson method was first used by Regge[18] and speculatively taken over into the domain of relativistic particle physics[19]. In the Regge theory[18], the partial wave expansion of the quantum mechanical amplitude ($f(\Theta)$) is replaced by a »finite« residue expansion at the poles of $S(l)$ ($= \mathrm{e}^{2i\delta_l}$) added to a background integral.

It should be remarked that the Regge poles can be derived, once a potential is given. This was discussed for heavy-ion scattering, in detail, by Tamura and Wolter[5] (T. W.). The T. W.[5] method was applied[8] to analyze the elastic scattering of $^{16}O + {}^{28}Si$ at $E_{lab} = 55$ MeV using different optical potentials (SD, GK, LC and E_{18} potentials). Among them the E_{18} potential does not produce fit to large angle data unless a Regge pole term is added in an ad hoc fashion. On the other hand, the LC potential is the most impressive, and fits the data quite well over almost the full angular range. This potential generates a number of poles (14 poles) in the first quadrant (physical region) of the complex l-plane. These poles exist in a region nearer to the real axis than are the poles generated from the other potentials. Near the grazing angular momentum ($l_g \sim 25$), the Regge pole with $\mathrm{Im}\, l \sim \sim 1.36 \pm 2$ is believed to be dominant scattering at backward angles. It is further seen that the real part of the LC potential has a »trapping region« in the neighborhood of the surface. On the other hand, the E_{18} potential has not a »trapping region«, neither generates that pole near the real axis, nor fits the data at backward angles. As a continuation and/or extension of $^{16}O + {}^{28}Si$ elastic scattering analysis to lower energies we used the conventional optical model potential[12], that was successful in getting reasonable fit to data particularly at low $E_{lab} = 33.16$ MeV in the search for the exact position of Regge poles and zeros.

3. *The deflection function $\Theta(l)$ and its behaviour near Regge poles*

The important connection between classical and quantum scattering results is best seen through the classical deflection function $\Theta(l)$, and its relation to the quantum phase shift. Many interesting cases appear in which: there is not a one-to-one relation between l and $\Theta(l)$; $\Theta(l)$ passes through $\pm\pi$ (glory effect), or $\Theta(l)$ possesses maxima, minima, or singularities for some angular momenta (rainbows or spiral scattering).

The deflection function is calculated from the relation

$$\Theta(l) = 2\frac{\mathrm{d}\,\delta_l}{\mathrm{d}l} = \frac{\mathrm{d}}{\mathrm{d}l}\,\mathrm{Re}\arg S(l). \tag{3}$$

It is convenient to note that the scattering matrix $S(l)$ (which is meromorphic) possesses two simple expansions[20] in terms of its poles (in the complex-plane). The first is the Mittag-Lefler expansion being used by Takemassa and Tamura[7] to investigate the roles of the pole-term and the corresponding background (term). The other expansion which we used in the present work is the product representation of the S-matrix. It has the double advantage of dealing explicitly with the zeros (in addition to poles) and of simply introducing a simple analytic formula for the deflection function $\Theta(l)$.

$S(l)$ is parametrized in terms of »pole-zero« factors as:

$$S(l) = S_l^0 \pi_n \frac{l - Z_n}{l - P_n}, \tag{4}$$

where $Z_n = l_{z_n} + \mathrm{i}z_n$ and $P_n = l_{p_n} + \mathrm{i}p_n$ are the zeros and poles. It is crucial that a good parametrization of the S-matrix has the same asymptotic functional behaviour for $l \to \infty$ and $l \to 0$ as the exact S-matrix. Equation (4) will be subjected to these constraints. The behaviour of $S(l)$ as $l \to \infty$ is such that each pole is associated with a zero (number of poles = number of zeros), thus $\lim_{l\to\infty} |\pi_n| \to 1$ and S_l^0 must be holomorphic (has no poles in the complex l-plane) and also tends to 1. On the other hand, the behaviour of $S(l)$ as $l \to 0$ ($|S(0)| \ll 1$) indicates that:

(a) For real potentials where the zeros are complex conjugates of the poles, thus $\lim_{l\to 0} |\pi_n| \to 1$ and thus $\lim_{l\to 0} |S(l)| \to S_l^0$. That is to say for real potentials, the background S_l^0 is the most important at $l \to 0$.

(b) For complex potentials (zeros and poles are not complex conjugates) $|Z_n| \neq |P_n|$ in general. If this situation is restricted by the condition $|Z_n| < |P_n|$ for all n thus the product $\pi_n \frac{l - Z_n}{l - P_n}$ could be made to tend to $S(l)$ as $l \to 0$.

$S(l)$ could be well approximated by

$$S(l) = \pi_n \frac{l - l_{z_n} - \mathrm{i}z_n}{l - l_{p_n} - \mathrm{i}P_n}. \tag{5}$$

From Eqs. (3) and (5), the complex deflection function could be represented in the complex Θ-plane by the relation

$$\Theta(l) = \mathrm{i}\sum_n \frac{1}{l - P_n} - \frac{1}{l - Z_n}. \tag{6}$$

It is to be noted that, summation in Eq. (6) is over all poles and zeros (typically 8 pole-zero pairs). Also, $\Theta(l)$ is a rational function and its denominator is a polynomial of degree $2n$, i. e., $\Theta(l)$ could not be approximated by l^{-1}.

On the real axis of the complex l-plane

$$\operatorname{Re}\Theta(l) = \sum_n \frac{Z_n}{(l - l_{z_n})^2 + \varepsilon_n^2} - \frac{P_n}{(l - l_{P_n})^2 + P_n^2}$$

$$\operatorname{Im}\Theta(l) = \sum_n \frac{l_{z_n} - l}{(l - l_{z_n})^2 + \varepsilon_n^2} - \frac{l_{P_n} - l}{(l - l_{P_n})^2 + P_n^2} \tag{7}$$

From Eqs. (7), it is clear that classical orbiting (singularity in $\Theta(l)$) occurs only for complex values of l, at the positions of Regge poles (and zeros). In other words complete orbiting never occurs for real values of l (unless $S(l)$ possesses a real zero).

On the other hand, it is known[14] that classical orbiting arises when the effective potential for the radial motion possesses, for some critical angular momentum l_c, a relative maximum (or minimum) equal to the available energy, mathematically expressed as:

$$V(r, l_c) = E \tag{8a}$$

and

$$\left(\frac{\mathrm{d}V}{\mathrm{d}r}\right)_{r_0} = 0. \tag{8b}$$

For complex potentials ($U_N = V_N(r) + \mathrm{i}W_N(r)$), Eq. (8a) cannot be satisfied unless l_c is complex (in agreement with the results obtained from semiclassical analysis (Eqs. (7)). Eqs. (8) is thus replaced by two equations:

$$E = V_c + V_N(r) + \frac{\operatorname{Re} l_c (\operatorname{Re} l_c + 1) - \varepsilon^2}{r_0^2} \frac{\hbar^2}{2\mu} \tag{9a}$$

and

$$(\operatorname{Re} l_c + 1/2)\,\varepsilon = -\frac{\mu}{\hbar^2} r_0^2 W_N(r_0) \tag{9b}$$

where

$$\varepsilon = \operatorname{Im} l_c.$$

From the last equation $\operatorname{Im} l_c$ ($=\varepsilon$) increases with increasing the imaginary depth of the nuclear potential. Comparing the results obtained from Eqs. (9) with that obtained from Eqs. (7) (describing the deflection function $\Theta(l)$), we can easily prove that only few Regge poles (or zeros) represent the critical angular momentum of orbiting, since Eqs. (7), (8) and (9) cannot be satisfied simultaneously at the position of each Regge pole.

4. *Results and discussions*

Results of the present search for position of Regge poles and values of their residues, using conventional optical model potential[12] (Table 1), and over the energy range 33.16 MeV $< E_{lab} <$ 55 MeV are given in Table 2. where ($\operatorname{Re} l_n = \lambda_n - 1/2$; $\operatorname{Im} l_n = \lambda_n$).

TABLE 1.

E_{lab} (MeV)	33.16	35.67	38.19	41.17	49.66	54.69
V_0 (MeV)	38.60	37.70	35.70	32.50	27.50	24.00
W_0 (MeV)	1.10	1.40	1.50	1.8	2.70	3.20

$r_0 = r_I = 1.36$ fm and $a_0 = a_I = 0.404$ fm.
Optical model parameters used in $^{16}O + {}^{28}Si$ BNL data.

TABLE 2.

$E_{lab} = 33.16$ MeV

n	$Re\lambda_n$	$Im\lambda_n$	$Re\beta_n$	$Im\beta_n$
0	20.67	0.40	0.00002	0.00004
1	17.54	0.40	0.001	0.003
2	14.74	0.42	0.016	0.074
3	12.24	0.59	0.036	0.420
4	9.76	0.87	0.28	0.97
5	7.31	1.07	1.12	1.27
6	4.96	1.17	2.24	0.94
7	2.73	1.19	3.15	0.28
8	0.62	1.16	3.73	−0.04

$E_{lab} = 41.17$ MeV

n	$Re\lambda_n$	$Im\lambda_n$	$Re\beta_n$	$Im\beta_n$
0	24.48	0.065	−0.0001	−0.0001
1	21.01	0.610	−0.02	−0.03
2	18.19	0.85	0.13	0.49
3	15.40	1.47	0.98	1.22
4	12.47	1.93	2.72	−0.53
5	9.65	2.16	0.28	−4.45
6	7.02	2.21	−6.59	−2.97
7	4.59	2.18	−9.89	5.60
8	2.34	2.11	−8.62	15.97

$E_{lab} = 35.67$

n	$Re\lambda_n$	$Im\lambda_n$	$Re\beta_n$	$Im\beta_n$
0	21.40	0.50	0.0002	0.0002
1	18.00	0.50	0.008	0.019
2	15.31	0.59	0.045	0.254
3	12.78	0.94	0.24	0.87
4	10.18	1.27	1.28	1.20
5	7.65	1.41	2.79	0.054
6	5.25	1.53	3.27	−2.47
7	2.98	1.53	2.58	−5.06
8	0.86	1.48	2.15	−6.93

$E_{lab} = 49.66$ MeV

n	$Re\lambda_n$	$Im\lambda_n$	$Re\beta_n$	$Im\beta_n$
0	25.30	0.89	0.02	0.01
1	22.37	1.19	0.29	0.66
2	19.30	2.25	1.86	0.89
3	15.89	2.96	1.06	−2.90
4	12.66	3.24	−4.30	0.70
5	9.72	3.30	4.45	5.40
6	7.04	3.23	7.61	10.77
7	4.60	3.12	−19.60	−20.32
8	2.33	2.97	−63.48	0.11

$E_{lab} = 38.19$ MeV

n	$Re\lambda_n$	$Im\lambda_n$	$Re\beta_n$	$Im\beta_n$
0	21.20	0.54	0.001	0.002
1	18.18	0.56	0.03	0.10
2	15.55	0.89	0.15	0.69
3	12.84	1.34	1.12	1.23
4	10.13	1.64	2.79	−0.29
5	7.5	1.78	1.96	−3.93
6	5.11	1.81	−2.43	−6.25
7	2.84	1.78	−7.89	−6.03
8	0.72	1.71	−11.68	−6.24

$E_{lab} = 55$ MeV

n	$Re\lambda_n$	$Im\lambda_n$	$Re\beta_n$	$Im\beta_n$
0	25.89	1.032	0.13	0.17
1	23.12	2.019	1.08	1.21
2	19.53	3.27	2.06	−1.62
3	15.84	3.83	−3.19	−0.41
4	12.51	3.97	3.47	2.63
5	9.54	3.92	−2.11	−7.36
6	6.86	3.79	−11.30	12.51
7	4.41	3.62	32.96	29.62
8	2.15	3.43	−124.7	−19.32

The positions and the residues of the Regge poles for the elastic scattering of $^{16}O + {}^{28}Si$.

Fig. 1 shows a display for the position of these Regge poles together with Regge zeros in the complex l-plane. At low energies (33.16, 35.67 and 38.19 MeV), the pole-zero trajectories in the Argand diagram look similar, however at higher

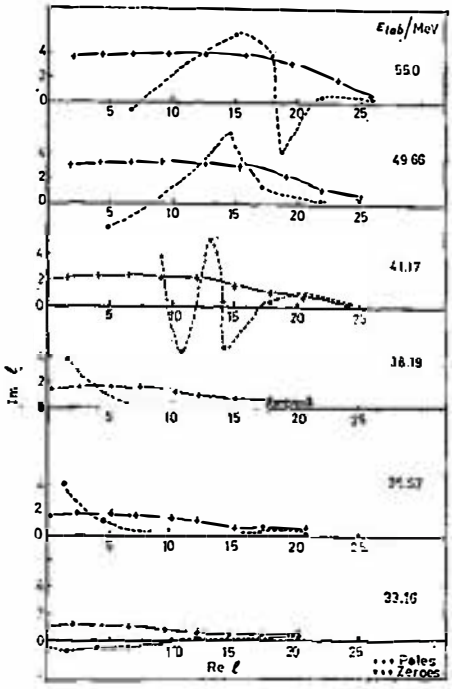

Fig. 1. Regge poles and zeros, of $^{16}O + {}^{28}Si$ elastic scattering S-matrix, presented in the complex l-plane, at different energies (using potential parameters of Table 1).

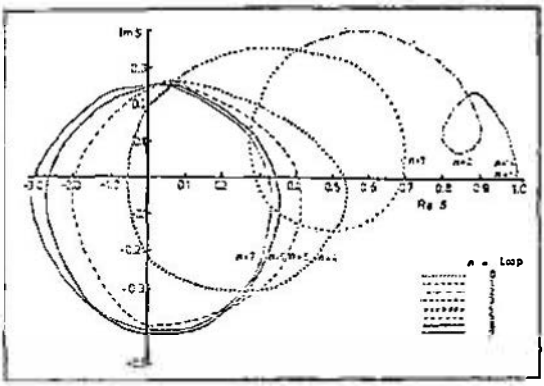

Fig. 2. The S-matrix of $^{16}O + {}^{28}Si$ elastic scattering at $E_{lab} = 33.16$ MeV, represented in the Argand diagram as l moves along the axis from 0 to ∞.

energies (41.17, 49.66 and 55 MeV) the ($n > 3$) zeros appear anomalously located (this is due to the anomalous values of residues at the corresponding poles). Moreover, some of these zeros exist so far from the real axis such that they may violate unitarity of $S(l)$. In Fig. 2, the S-matrix (at $E_{lab} = 33.16$ MeV) is represented in the Argand diagram. It contains a number of loops, each loop corresponding to a single »pole-zero« factor. The $S(l)$ travels around a »resonance loop« beginning at $l = l_{P_8}$, encircling the origin in the clockwise direction and crosses the imaginary axis as l

approaches the next pole (l_{p7}, l_{p5}, l_{p3}, l_{p4}), that is, these resonances are predominantly elastic[21]. The resonance loops n_0, n_2 and n_1, do not encircle the origin (predominantly inelastic).

4—1. Pole zero decomposition of $\Theta(l)$

In Fig. 3 the results of exact numerical calculations of the real part of $\Theta(l)$ from Eq. (3) at $E_{lab} = 33.16$ MeV, are compared with the results obtained from the

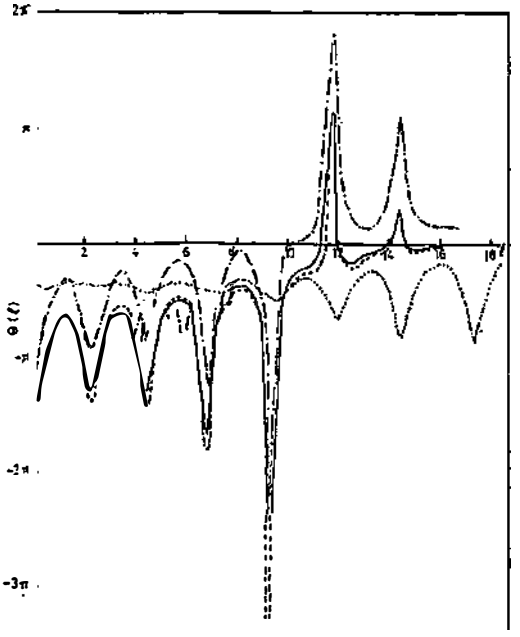

Fig. 3. The numerically calculated deflection function $\Theta(l)$ (solid curve) using equation (3) is compared with that calculated from the analytic formula (Eq. (7)) (dashed curve). The figure shows also the dominance of Regge zeros (dashed-dotted curve) rather than Regge poles (dotted curve).

corresponding analytical formula Eq. (7). The close agreement between them is a justification for the latter. Also shown in Fig. 3, the pole-zero decomposition of $\Theta(l)$ which demonstrates the more effective role of Regge zeros relative to Regge poles for all values of l's. Thus the deflection function if governed much more by Regge zeros than by Regge poles simply because both are singularities of $\Theta(l)$ and the zeros are closer to the real axis than the poles. This is specially true at energies in the resonance range occuring in a narrow band of l values near $l \simeq KR$.

4—2. Rainbow features

Resonance loops that appeared in Fig. 2 are now displayed on $\Theta(l) - l$ plane (Fig. 4) as number of spikes describing several resonances. In Fig. 4, the zeros labelled by $n = 0$, 1, 2 and 3 have clearly crossed into the upper half plane, giving maxima in $\Theta(l)$, but haven't yet been »annihilated« by meeting their poles except

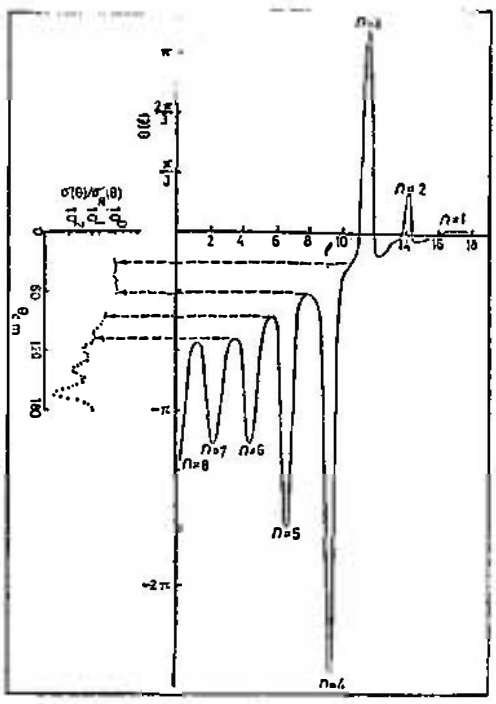

Fig. 4. The real part of the deflection function $\Theta(k)$ as a function of l at $E_{lab} = 33.16$ MeV. Also shown in the figure the experimental $^{16}O + ^{28}Si$ elastic scattering cross sections data[2,3].

for $n = 0$ where the value of residue is nearly zero (Table 2). The remaining zeros, for lower l are what produce the deep minima in the deflection function. A number of rainbows $\left(\frac{d\Theta(l)}{dl} = 0\right)$ appear near l-values between consecutive zeros. These

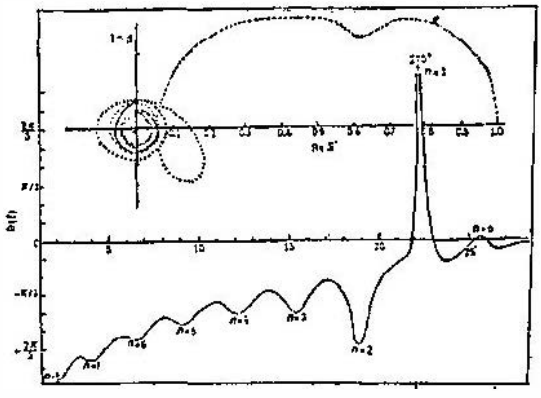

Fig. 5. The same as Figs. 2 and 4, but at $E_{lab} = 55$ MeV.

rainbows are presumably corresponding to maxima in the experimental $^{16}O + {}^{28}Si$ elastic scattering cross section at that energy (33.16 MeV). Because the deep minima in $\Theta(l)$ distinctly come from the zeros rather than the (more distant) poles it appears they have an almost no significant influence on the cross section. However, the presence of a »zero-pole« in nuclear diagonal S-matrix revealed a crucial role for zero position relative to the pole position in describing the anomalous large angle α-particle scattering from calcium isotopes[22]. At higher energy (55 MeV) a similar shape of $\Theta(l) - l$ is obtained (Fig. 5), however, the variation of $\Theta(l)$ is more smooth at lower l-values (resonances overlap) except near $l = 22$, indicating that resonance effects disappear at higher energies.

4—3. Orbiting features

As can be seen from Fig. 4, orbiting ($\Theta < -2\pi$) occurs at l values where $\Theta(l)$ changes its sign from negative to positive (indicating change from attractive potential to repulsive). This orbiting appears to be caused by the existence of a zero in the

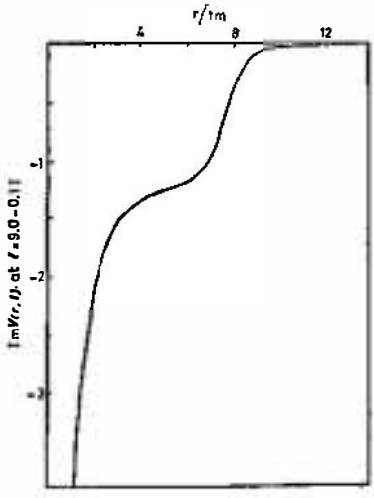

Fig. 6. The imaginary potential at $E_{lab} = 33.16$ MeV at the complex value $l = 9 - 0.1$ i (zero nearest to the real axis).

fourth quadrant just below the real axis ($z = 9 - 0.1i$). In terms of potentials this zero corresponds to a strong imaginary centripetal potential singular at the origin (Fig. 6),

$$\text{Im } V(l,r) = W_N(r) + \frac{\hbar^2 (2l+1)\varepsilon}{2\mu \quad r^2}. \tag{10}$$

At $l = z_4 = 9 - 0.1i$, the S-matrix drops to zero, indicating complete absorption, and from Eq. (10), the imaginary (absorbing) potential is increased by the centripetal part $\frac{\hbar^2}{\mu} \frac{(9.5)0.1}{r^2}$ which tends to $\to \infty$ as $r \to 0$.

On the other hand, as l moves in the upper half of the complex-plane (positive imaginary part) then from Eq. (10) the imaginary part of the potential becomes singular positive at the origin (emitting instead of being absorptive). This in fact does not have a clear physical meaning, because the S-matrix is non unitary in a large domain of the upper half of the complex l-plane.

4—4. Effect of real/imaginary potential strength

We consider first the case of real potential ($W = 0$). In a band of l-values ($l > KR$); $12 < l < 26$ at $E_{lab} = 33.16$ MeV ($E_{cm} = 21.1$ MeV) and $25 < l < 27$ at $E_{lab} = 55$ MeV ($E_{cm} = 35$ MeV) the real potential has a pocket at these

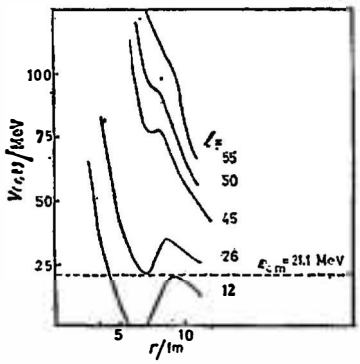

Fig. 7. Effective real potential for different l values using optical model parameters of Table 1. A display for the band of l-values ($12 < l < 26$) is also shown at $E_{cm} = 21.1$ MeV. The potential pocket disappears at $E_{cm} > 94$ MeV.

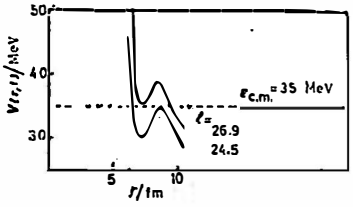

Fig. 8. The same as Fig. 7 with a display for l-values ($25 < l < 27$) at $E_{cm} = 35$ MeV.

energies (Figs. 7, 8). The pocket disappears at $E_{cm} > 94$ MeV ($E_{lab} > 147$ MeV). Regge poles with small real part are corresponding to resonances in lower partial waves, but for these partial waves the barrier top is below E, so that poles correspond to broad overlapping resonances (with $2\mathrm{Im}\,\lambda_n > \mathrm{Re}\,(\lambda_n - \lambda_{n-1})$) giving rise to smooth deflection function for small l's as shown in Fig. 9.

Effect of the imaginary potential strength will be considered as the direct display for the connection between singularities of the scattering matrix and properties of the cross section in a more clear and reliable fashion. The strength of the imaginary part of the potential (W) was increased from 1.1 MeV to 10 MeV (more absorption is added), that will of course move Regge poles (and accordingly zeros) »up« in the l-plane, i. e., increasing their imaginary parts (P_n and Z_n). Shown in

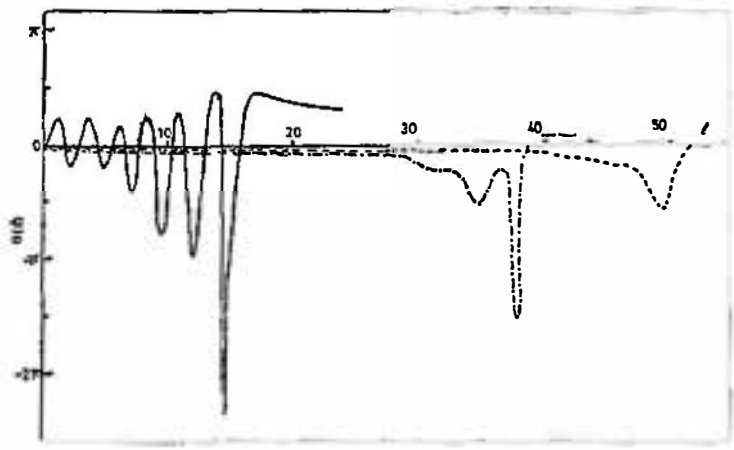

Fig. 9. Deflection function $\Theta(l)$ (including Coulomb effects) for real potentials at three different energies; $E_{lab} = 33.16$ MeV (solid line), 94 MeV (dashed-dotted) and 147 MeV (dotted line).

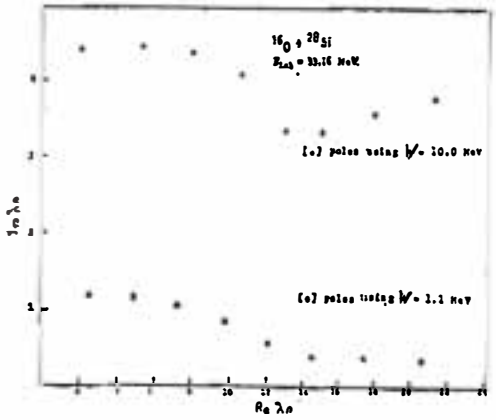

Fig. 10. Positions of Regge poles derived at $E_{lab} = 33.16$ MeV using potential parameters of Table 1 with (a) $W = 10$ MeV and (b) $W = 1.1$ MeV.

Fig. 10 Regge poles that are dramatically shifted away from the real axis causes these poles not to have the properties of resonances in the usual sense as can be seen from Eq. (7). Of course one would not expect the theoretically calculated cross section to properly fit the corresponding experimental data. This is shown in Fig. 11 where $\sigma(\Theta) = \sigma_R(\Theta)$ shows a rapid (structureless) fall off beyond $\Theta_{cm} = 90°$ and the quality of fit was considerably worsened.

4—5. Nearside/farside decomposition of the angular distribution

In WKB terms, there is only one »inner« radial turning point for each lower l-partial wave, and these small-l rays (farside, of course) are evidently being described by overlapping Regge poles and affecting the farside of the cross section. Although the deep minima in the deflection function (Fig. 4) considered as have

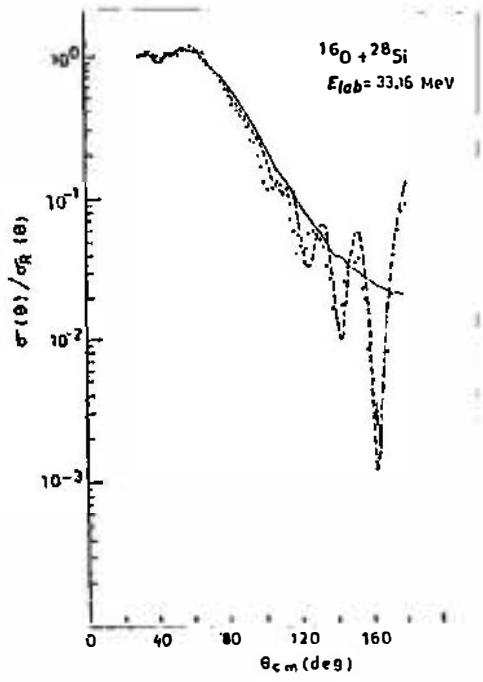

Fig. 11. Elastic scattering cross section of $^{16}O + ^{28}Si$ at $E_{lab} = 33.16$ MeV. Data are of Braun-Munzinger et al.[2,3]. The solid and dotted lines are the theoretically calculated cross section using potential parameters of Table 1, with $W = 10$ MeV and 1.1 MeV, respectively.

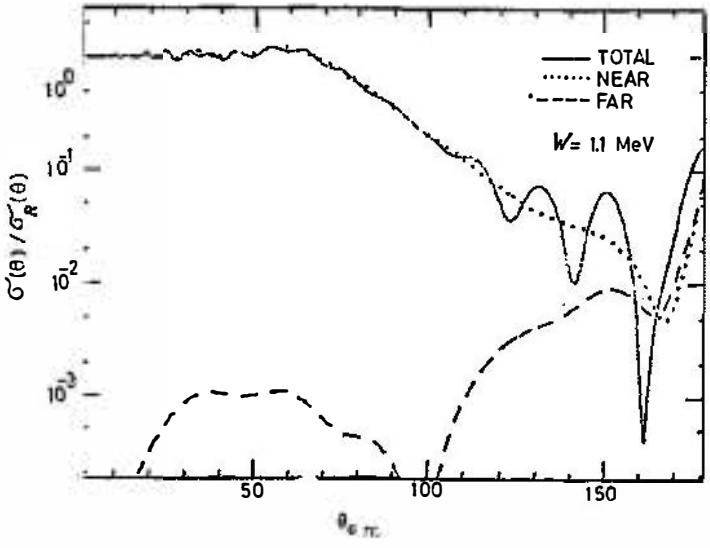

Fig. 12. Nearside/farside decomposition of cross section, at $E_{lab} = 33.16$ MeV using $W = 1.1$ MeV.

an almost no significant influence on the cross section, they will in any case influence the farside cross sections. Hence the deflection function, for a real potential (which seems a better guide to physics) describes, except for the last few high l-values, just a simple »classical« rainbow-type deflection function; the deep minima in the far-side cross section at 100° and 165° (Fig. 12) are in this interpretation, viewed as the

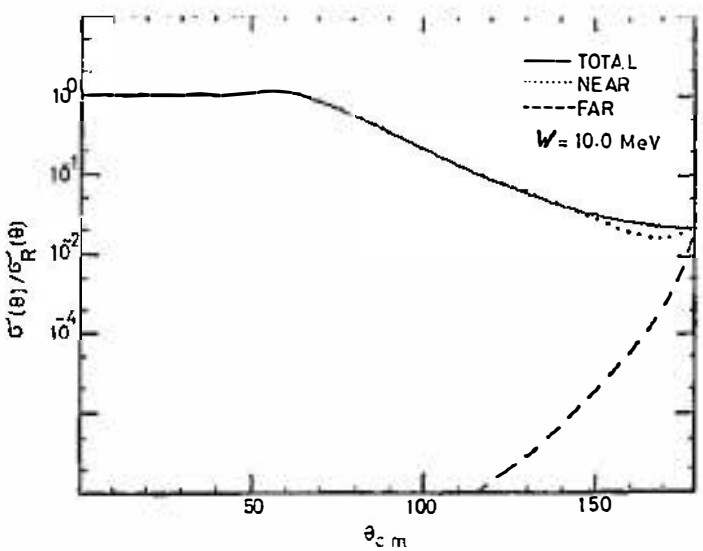

Fig. 13. The same as Fig. 12 but using $W = 10$ MeV.

bright-side »airy« minima of this rainbow. With Regge poles shifted away from the real axis, particularly for low l-values (Fig. 10), losing their resonance properties, the contribution of the nearside cross section became the dominant one with an almost negligible contribution from the farside cross section (Figs. 12 and 13).

5. *Conclusion*

We have tried to explore the key physical process that is occurring in $^{16}O + {}^{28}Si$ elastic scattering via search for the exact position of the Regge poles of the S-matrix (Table 2), parametrization of the S-matrix in terms of these singularities (Eq. (4)) and a study for the behaviour of the corresponding analytical deflection $\Theta(l)$ (Eq. (7)). Rainbow features $\left(\frac{d\Theta(l)}{dl} = 0\right)$ that appear near l-values between consecutive zeros are presumably corresponding to maxima in the experimental $^{16}O + {}^{28}Si$ elastic scattering cross section (Fig. 4). The observed orbiting phenomenon ($\Theta(l) < -2\pi$, for l-values where $\Theta(l)$ changes its sign) is found to be caused by a pole of negative order (zero) just below the real axis ($Z = 9 - 0.1i$) and is explained by strong imaginary centripetal potential (Eq. 10) singular at the

origin (Fig. 6). Also $\Theta(l)$ shows, for real nuclear potential (Figs. 7 and 8), how resonance phenomena at low energies become rainbows at higher energies (Fig. 9).

A better physical insight into $^{16}O + {}^{28}Si$ scattering mechanism was also revealed by establishing a direct connection between position of Regge poles and features of the cross section. We have shifted the position of Regge poles away from the real axis (Fig. 10) by increasing the strength of the absorptive part of the nuclear potential (increasing W). This causes Regge poles not to have the properties of resonances in the usual sence as can be seen from Eq. (7). The corresponding theoretical cross section shows a rapid (structurless) fall off beyond $\Theta_{cm} = 90°$ and its quality of fit to the corresponding experimental data (Fig. 11) was considerably worsened. With this shift of Regge poles (particularly for low l-values) the contribution of the nearside cross section became the dominant one with an almost negligible contribution from the farside cross section (Figs. 12 and 13).

Acknowledgment

The authors would like to express their deep appreciation to Prof. G. R. Satchler of ORNL and Prof. K. McVoy of Phys. Dept. Wisconsin University for carrying on the present nearside/farside calculations and for their continuous help and fruitful discussions. The kind hospitality of both ORNL and University of Wisconsin is highly appreciated.

References

1) P. Braun-Munzinger, G. M. Berkowitz and T. M. Cramer, Phys. Rev. Lett. **38** (1977) 944;
2) C. K. Gelbke, T. Awes, U. E. P. Berg, M. J. LeVine and P. Braun-Munzinger, Phys. Rev. Lett. **41** (1978) 1778;
3) P. Braun-Munzinger, G. M. Berkowitz, M. Gai and C. M. Jackcinski, Brookhaven National Laboratory (BNL) Report No. 28405; Phys. Rev. **C24** (1981) 1010;
4) V. Shkolnik and D. Dehnhard, Symposium on Heavy Ion Elastic Scattering, University of Rochester (1977), unpublished; M. Golin and S. Kahana, Symposium on Heavy Ion Elastic Scattering, University of Rochester (1977), unpublished; S. Y. Lee and Y. D. Chan, University of Washington Report No. 1388 (1977) 743, unpublished;
5) S. U. Lee, Nucl. Phys. **A311** (1978) 518; J. Barette and S. Kahana, Nuclear and Particle Physics **9** (1980) 67;
6) D. Dehnhard, V. Shkolnik and M. A. Franey, Phys. Rev. Lett. **40** (1978) 1549;
7) M. C. Mermaz, Phys. Rev. **C23** (1981) 755; T. Takemassa and T. Tamura, Phys. Rev. **C18** (1978) 1282;
8) T. Tamura and H. H. Wolter, Phys. Rev. **C6** (1972) 1976;
9) A. M. Kobos, G. R. Satchler and R. S. Mackintosh, Nucl. Phys. **A395** (1983) 248;
10) S. Kahana, J. Barette, B. Berthiet, E. Chavez, E. Greines and M. C. Mermaz, Phys. Rev. **C28** (1983) 1393;
11) M. C. Mermaz, E. R. Chavez-Lomeli, J. Barette, B. Berthier and A. Greiner, Preprint, DPH-N/BE, CEN Saclay, 91191 Gif-sur-yvette Cedex, France (1983);
12) M. Shalaby, A. El Naiem, H. Khalil and M. Abdel Keriem, Physica Scripta **27** (1983) 393;
13) C. S. Shastry and I. Parija, Phys. Rev. **C27** (1983) 2042;
14) K. W. Ford and J. A. Wheeler, Ann. of Phys. **7** (1959) 287;
15) H. Poincaré, Rend. Circ. Math. Palermo **29** (1910) 169;
16) J. W. Nicholson, Phil. Mag. **19** (1910) 516; **20** (1910) 157;

17) G. N. Watson, Proc. Roy. Soc. **95** (1918) 83;
18) T. Regge, Nuovo Cim. **14** (1959) 951;
19) G. F. Chew and S. Frauschi, Phys. Rev. Lett. **5** (1960) 580; G. F. Chew, *Theory of Strong Interactions*, W. A. Benjamin (New York, 1961);
20) R. G. Newton, *The Complexj-Plane*, W. A. Benjamin (New York, 1964);
21) K. W. McVoy, Phys. Rev. **C3** (1971) 1104;
22) A. Y. Abul Magd, H. M. Khalil and M. M. Shalaby, Z. Physik **A281** (1977) 57.

POLUKLASIČNA I KVANTNO-MEHANIČKA ANALIZA ELASTIČNOG RASPRŠENJA $^{16}O + {}^{18}Si$

HALA M. KHALIL

University College for Girls, Ain Shams University,

Heliopolis, Cairo, Egypt

MOSTAFA M. SHALABY and M. ABD EL-KERIEM

Ain Shams University, Faculty of Science, Phys. Dept., Cairo, Egypt

UDK 539.17

Originalni znanstveni rad

Istraživani su Regge polovi i pripadni reziduumi S-matrice za elastično raspršenje $^{16}O + {}^{18}Si$ za konvencionalni optički potencijal u rasponu energija 33,16 MeV$\leq E_{lab} \leq$55 MeV. Funkcija otklona je nađena iz parametrizacije S-matrice pomoću Regge polova i utvrđeno je da se struktura u elastičnom udarnom presjeku može objasniti orbitiranjem i dugom. Orbitiranje se objašnjava Regge polom s negativnim imaginarnim dijelom.